# Surface states governing activity and selectivity of Pt-based ammonia slip catalysts for selective ammonia oxidation

Vasyl Marchuk,*[a] Dmitry I. Sharapa,[b] Jan-Dierk Grunwaldt, [a,b] and Dmitry E. Doronkin*[a,b]

[a.] *Institute for Chemical Technology and Polymer Chemistry (ITCP), Karlsruhe Institute of Technology, Engesserstr. 20, 76131 Karlsruhe, Germany.*

[b.] *Institute of Catalysis Research and Technology (IKFT), Karlsruhe Institute of Technology, Hermann-von-Helmholtz-Platz 1, 76344 Eggenstein-Leopoldshafen, Germany.*

*E-mail: vasyl.marchuk@kit.edu, dmitry.doronkin@kit.edu*

**Abstract**

Selective oxidation of ammonia to nitrogen over $Pt/Al_2O_3$ was studied in order to determine active Pt species for the activity and selectivity of Pt under conditions close to realistic emission control applications. For this purpose, reaction rates and apparent activation energies were measured at different compositions of the reaction feed. Additionally, *in situ* diffuse reflectance infrared Fourier transform spectroscopy (DRIFTS) and *operando* X-ray absorption spectroscopy (XAS) including its interpretation based on theoretical XAS calculations were applied. Three main chemically different states of Pt were detected. The predominance of each of them correlated with the different performance of the catalyst at distinct temperature ranges. At low temperatures (<150 °C) Pt surface was covered by oxygen species which poisoned the catalyst. They needed to be removed by heating in reaction mixture to start with a light off. At 150 – 300 °C, Pt was covered with $NH_x$ species which provided the maximal selectivity to $N_2$. At higher temperatures, when full ammonia conversion was reached, the Pt surface again became available for oxidation by O-species resulting in both surface chemisorbed and subsurface O. This high-temperature state possessed high oxidation activity and high selectivity to undesired $N_2O$ and $NO_x$.

Keywords: renewable ammonia, selective catalytic oxidation, emission control, *operando* spectroscopy, XANES calculations

## 1. Introduction

Ammonia is one of the perfect candidates to become a sustainable energy carrier in the future carbon-neutral economy.[1-4] It can be compressed and liquefied much easier than hydrogen, and its liquid state has higher energy density.[1, 2] This simplifies storage and transportation and makes it readily available for use in fuel cells as is, cracking it to back hydrogen, or simple combustion in gas turbines or internal combustion engines.[4, 5] Usually, in all these applications ammonia consumption is incomplete. Therefore, its slip into atmosphere is imminent and, as a toxic and greenhouse gas, it needs to be removed. An efficient approach to eliminate ammonia is using ammonia slip catalysts (ASCs) that selectively convert this pollutant to nitrogen and water.[6, 7]

ASCs are typically based on noble metals, mostly platinum as an efficient oxidation catalyst.[8-10] They are known in automotive industry at the final stage of diesel exhaust treatment. In this case, they are used to eliminate unreacted ammonia that is dosed as a reductant of $NO_x$ in selective catalytic reduction (SCR) system.[9, 11] The driving force to improve ASCs is to increase their activity at low temperatures occurring e.g. during a cold start of an engine or to remove ammonia slipped from fuel cells. Another problem of ASCs is that, in spite of high activity, at elevated temperatures they produce undesired $N_2O$ and NO as the main products.[10, 12, 13] Understanding the factors, which govern activity and selectivity of ASCs, is necessary for further improvement of their performance.

A number of groups conducted fundamental studies on ammonia oxidation mechanism. Some were based on DFT calculations [14-18] and experiments on single crystals[18-22]. Considering the fact that real catalysts expose a variety of crystal facets, other studies addressed the reaction mechanism using platinum gauzes[18, 23-25], polycrystalline Pt[21, 26-28] and supported Pt[29, 30]. In these works the gradual hydrogen cleavage from ammonia as rate-limiting step as well as the influence of surface coverages of adsorbates on selectivity were discussed.

However, most of the experiments in these fundamental studies were performed at conditions far from real applications. Many tests were conducted under high vacuum which alters catalyst performance compared to atmospheric pressure. For example, at decreased pressure almost no $N_2O$

is formed, while at atmospheric pressure it is a plentiful undesired byproduct.[18, 21] Moreover, oxides, which are formed on platinum during catalyst preparation and after contact with ambient air, play an important role in real ASCs performance [31-33], but can be only studied to a limited extent under high vacuum conditions. In addition to this pressure gap, also the material gap needs to be bridged. Particularly important is the study of ammonia oxidation catalysts over supported Pt particles, since support may interact either with Pt, stabilizing particles of certain size and shape, or with reactants and products, for example, storing ammonia and thus directly changing catalyst performance.[29, 34-37]

Recent progress has allowed bridging the pressure and material gaps by using supported platinum particles and increasing reactant pressure several orders of magnitude above the pressures of ultrahigh vacuum. *In situ* and *operando* near-ambient pressure (NAP) XPS was used to follow the surface state of platinum in reacting gas mixture in the millibar pressure range.[18, 19, 21, 26, 36, 38, 39] These studies revealed the types and nature of the adsorbates on Pt surface in reactive gas environment, their change with temperature, and the role of surface coverages in reaction selectivity. These were mainly ammonia, its dissociation products, and surface oxygen-containing species. However, the partial pressures used in these studies are still significantly lower than in real applications. Hence, they do not allow to fully examine the impact of reacting conditions on Pt oxide formation, and only a limited amount of platinum oxide was observed.[19, 38] Thus, its role in the reaction mechanism could not be unraveled. We further reported the oxide decomposition to be required for reaction initiation.[36] This decomposition was achieved through an additional reduction step. Hence, it would be necessary to verify whether the same effect occurs under realistic reaction conditions.

Other works approached the more realistic conditions of ammonia oxidation via testing supported platinum at atmospheric pressure. For example, the studies of structure sensitivity under these conditions demonstrated increasing reaction rate for larger Pt particles and reduced catalysts.[40-43] Furthermore, kinetic models were developed based on mechanistic reaction networks to predict catalyst performance under application-relevant conditions.[10, 12, 33, 44, 45] Another study under realistic conditions by Ghosh et al.[33] outlined the role of Pt surface step crystal planes and platinum oxide. They

additionally found that high ammonia concentrations led to Pt deactivation, in line with studies reporting inhibition with surface nitride formation in the excess of ammonia.[28, 30] The role of surface restructuring was also reported in studies [18, 21]. Nevertheless, the works mentioned above and performed under application-relevant conditions do not directly probe the state of Pt during the reaction. Unravelling the state of supported Pt under the atmospheric pressure was addressed by applying X-ray absorption spectroscopy (XAS),[32, 36] which is capable of tracking catalyst state during its operation at relevant pressures and temperatures.[46-49] Nonetheless, when standard *operando* XAS was used, the spectral changes of Pt were too subtle to be resolved.[36] A progress was achieved by applying quick-scanning extended X-ray absorption fine structure spectroscopy (QEXAFS) which had higher sampling rate.[32] Still, the authors determined only the oxidation state of Pt using Pt and $PtO_2$ as references and noted that the experimental spectra could not be precisely described only by these two states as the coordination environment of the studied samples was more complex.[32] The surface species that could be present on Pt under atmospheric pressure and reaction conditions were not analyzed. Therefore, it is required to complement these results by describing the possible reference states of Pt with types of adsorbates which could occur in realistic ASC operation.

The aim of this work was to examine the change of Pt state in alumina-supported ASCs under reaction conditions relevant for exhaust gas aftertreatment and to compare them with the previously reported results in order to bridge the pressure and material gap in understanding of this system. This was achieved by using *operando* XAS around the Pt $L_3$-edge, i.e. the X-ray absorption near-edge structure (XANES). Identification of the Pt states was assisted by kinetic studies, *operando* diffuse reflectance infrared Fourier transformed spectroscopy (DRIFTS) and calculations of the XANES spectra. The results improve understanding of real industrial catalyst transformations under reaction conditions and factors influencing their activity and selectivity. These findings would assist rational design of ASCs with improved characteristics.

## 2. Experimental details

### 2.1 Catalysts preparation and characterization

Two 2 wt. % Pt/γ-$Al_2O_3$ catalysts were prepared with incipient wetness impregnation (IWI). First, γ-alumina (Sasol SCFa-230) was calcined at 750 °C for 4 h in air. Then it was impregnated with a solution of Pt (II) nitrate (Chempur, anhydrous, 99.95 %), dried in air for 40 h at room temperature and further for 1 h at 60 °C. The impregnated catalyst was calcined in static air at 400 °C and then reduced in $H_2$ flow at the same temperature. To obtain catalysts with Pt nanoparticles of different sizes, one part of the reduced sample was additionally calcined at 500 °C and another – at 700 °C with no further treatment in both cases. The first catalyst will be further referred to as PtA-IW-500, and the second – PtA-IW-700.

The catalysts were characterized with high-angle annular dark-field scanning transmission electron microscopy (HAADF-STEM) and *ex situ* extended X-ray absorption fine structure spectroscopy (EXAFS) and the results are reported elsewhere.[50] TEM demonstrated a broad particle size distribution in PtA-IW-700 with the average particle size of 13.6 nm, supported by the EXAFS-derived average coordination number of about 12 typical for bulk platinum metal. Two main fractions of Pt species in the PtA-IW-500 were detected with TEM: nanoparticles of 1.8 nm average diameter and a highly dispersed fraction consisting of clusters of different sizes, from single to tens of atoms. The average coordination number of Pt of 4.3 ± 1.7, based on *ex situ* EXAFS, corresponded to clusters of 0.5-1 nm diameter.[51]

### 2.2 Catalytic tests

Temperature-programmed tests were conducted in a plug-flow tubular quartz reactor. The reaction feed contained 500 ppm $NH_3$ and 13 % $O_2$ in $N_2$ with total gas flow 1050 $cm^3$/min. Two cycles of heating from 50 °C to 400 °C and cooling down to 50 °C with 3 °C/min ramp rate were performed. The first cycle was used for catalyst pre-treatment to obtain a stable form of the samples that gives reproducible results under the tested environment. Very similar conversion profiles obtained for the

first and the second cooling in the reaction mixture (fig S1) demonstrate that stable catalysts were formed already after the first heating cycle. The results of the second catalytic cycle are reported in this study. The resut The catalytic results obtained light off and light-out The catalysts loading amounted to 25 mg. A sieve fraction with grain size 100-200 µm was used. The catalysts were diluted with silicon carbide (same sieve fraction) to reach a catalyst bed volume corresponding to 63,000 $h^{-1}$ of gas hourly space velocity. Effluent gas mixture was analyzed with a MultiGas 2030 FTIR spectrometer (MKS Instruments, USA). The conversion of ammonia ($X_{NH_3}$) was calculated with $X_{NH_3} = (1 - C_{NH_3}^{out}/C_{NH_3}^{in}) \cdot 100\ \%$, where $C_{NH_3}^{out}$ and $C_{NH_3}^{in}$ are ammonia concentrations on reactor outlet and inlet respectively. Product selectivities were calculated as $S_i = n_i \cdot C_i\ /(C_{NH_3}^{in} - C_{NH_3}^{out}) \cdot 100\ \%$, where $C_i$ is product $i$ concentration and $n_i$ – number of nitrogen atoms in the product molecule. The nitrogen concentration was derived from the mass balance, taking into account total ammonia consumption and concentrations of other products.

Integral chemical reaction rates for kinetic analysis were determined by calculating the amount of converted ammonia (in mmol) per minute per a gram of Pt metal. Ammonia or oxygen concentrations were varied while the concentration of the second component was kept constant. The concentrations used for the analysis were taken after establishing equilibrium which took between 30 and 120 min.

For determining apparent activation energies, heating and cooling at varied reactant ratios and different partial pressures of oxygen were conducted. These tests were made on PtA-IW-700. The reaction mixtures used for the comparison of different $NH_3$:$O_2$ ratios were 13 % $O_2$ with either 500 or 1000 ppm $NH_3$. The reaction mixtures used for different oxygen partial pressures comparison were: 100 ppm $NH_3$ with 1.3 % $O_2$; 200 ppm $NH_3$ with 2.6 % $O_2$; 1000 ppm $NH_3$ with 13 % $O_2$. For apparent activation energy calculation in different reaction mixtures, 4 temperature points with $NH_3$ conversions in the range of 2.5-10 % were used. To exclude the influence of intraparticle mass transfer limitations on the measured apparent reaction rate, the compliance to Weisz-Prater criterion was inspected.[52] Particularly, it was shown that the difference between the efficient and intrinsic reaction rates did not

exceed 10 %. This indicates a negligible effect of intraparticle diffusion on the reaction rate. The respective estimations are provided on pp. S1-S2 of the Supporting Information (SI).

2.3. *Operando* DRIFTS studies

A VERTEX 70 Fourier transform infrared spectrometer (Bruker Optics, Germany) with a mercury cadmium telluride detector was used to measure *operando* DRIFTS spectra. The spectrometer was equipped with Praying Mantis diffuse reflection optics and a high temperature cell (Harrick) with a home-made dome with a flat $CaF_2$ window. The cylindrical sample-containing compartment of the cell was completely filled with 60 mg of PtA-IW-700 sample with 100-200 µm grain size fraction. The composition of the reaction mixture was 500 ppm $NH_3$ and 10 % $O_2$ in He. The gas flow of 100 $cm^3$/min was flushed from the top to the bottom of the catalyst bed.

The sample was heated in He to 400 °C and cooled down stepwise to room temperature in the same atmosphere. 30-minute-long temperature steps at 400, 300, 250, 200, 150, 100 °C were made. Reference spectra in He were measured at the end of each temperature step. After this the sample was cooled down to 50 °C and kept for 30 min. This was followed by switching to the reaction mixture and 30 min of equilibration. Then stepwise heating in the reaction mixture started with the same temperature steps as during cooling in He. The sample was maintained for 30 min at each temperature step in the reaction mixture, which was followed by recording DRIFTS spectra.

For online analysis of outlet gas composition, an Omnistar GSD-320 quadrupole mass spectrometer (Pfeiffer Vacuum GmbH) was used. To calculate conversion and product yields, relative concentrations of ammonia and reaction products were used. They were estimated based on minimum and maximum ion currents of each component normalized by ion current of He and taken as 0 and 1, respectively. The detailed quantification approach of the mass spectrometry data is descried on p. S3-S4 of the SI. The approach was used to follow the trends in surface species distribution detected by DRIFTS and the highest and the lowest products / educts concentrations which was done in the study.

2.4. *Operando* XAS studies

QEXAFS spectra at the Pt $L_3$ absorption edge were recorded in transmission geometry at P64 beamline of the PETRA III synchrotron radiation source (DESY, Hamburg, Germany).[53] Fast oscillating Si(111) channel-cut monochromator was used for scanning X-ray energy at a 5 Hz frequency. The sampling rate of ionization chamber detectors was 1 MHz. Higher harmonics were rejected by using a Rh-coated stripe on a pair of 800-mm-long Si mirrors. A beam size was set to 1 x 1 mm. The spectra of the samples were normalized and energy corrected in *ProQEXAFS v. 2.43* software.[54] *SIMPLISMA*[55] and multivariate curve resolution alternating least squares (MCR-ALS)[56] algorithms, integrated in this software, were applied for extracting individual spectral components of the recorded QEXAFS spectra. Further, with the help of the same program, linear combination analysis (LCA) was performed using the extracted spectral components as references.

The experiments were conducted on *in situ* setup, similar to the one described in reference [57]. The catalysts used were 100-200 µm sieved powders. They were loaded into 1.5 mm (outer diameter) quartz capillary microreactors with 0.02 mm wall thickness with a catalyst bed length of approximately 5 mm. An ammonia oxidation reaction mixture or gas mixtures containing reaction educts / products were dosed through the capillary microreactor. X-ray beam was probing the catalyst perpendicularly to the capillary in the point of the first third of a catalyst bed.

The reaction mixture for catalytic experiments feed contained 500 ppm $NH_3$, 10 vol. % $O_2$ balanced with He with a total gas flow of 75 $cm^3$/min. The samples underwent heating, cooling, and another heating in the reaction mixture from 50 to 400 °C and back with the rate 5 °C/min. The first heating and cooling in the reaction mixture were used for catalyst pretreatment. The results for the second heating cycle are presented.

After the catalytic experiments in the reaction mixture, the PtA-IW-500 sample was additionally heated from 50 to 400 °C with the heating rate 10 °C/min in He. Later, it was quickly cooled down to 50 °C, and the procedure was repeated in the atmospheres of different reaction educts / products in the following order: 500 ppm $NH_3$ in inert; 500 ppm NO in inert; 500 ppm NO and 10 % $O_2$ in inert; 10

% $O_2$ in inert. In parallel, QEXAFS spectra were recorded. The total gas flow amounted to 75 $cm^3$/min for every gas mixture.

Gas mixture on the reactor outlet was analyzed with a MultiGas 2030 FTIR spectrometer (MKS Instruments, USA).

2.5. XANES calculations

Density functional theory (DFT) calculations were conducted to determine the lowest-energy geometries of different adsorbates on Pt and species in its subsurface. These optimized geometries were used to calculate X-ray absorption near edge structure (XANES) spectra of platinum to further compare them with the experimental ones.

The DFT calculations were carried out using the Vienna Ab Initio Simulation Package (VASP)[58, 59] employing the generalized gradient approximation (GGA) with Bayesian error estimation functional with van der Waals corrections (BEEF-vdW)[60, 61] and the projector-augmented wave (PAW) potentials.[62, 63] A four-layer slab of platinum was used; during the relaxations the two bottom layers of the slabs were fixed. A kinetic energy cutoff of 450 eV was always used for the calculations. In order to avoid interaction between periodic images, the Pt slabs were separated by approx. 20 Å of vacuum along the *z*-direction. The files with atom coordinates of the optimized structures in *xyz*-format are available in ref. [64].

To calculate the X-ray absorption near edge structure (XANES) spectra of the models optimized with DFT, multiple scattering FEFF 9.6.4 *ab initio* code[65] was used. Radii for full multiple scattering and the self-consistent potential calculations were 5 Å in both cases. For high energy resolution, the line broadening was reduced by applying the value of (-1.6) eV to vi0 in the EXCHANGE card.[66] XANES calculations were performed for Pt atoms in non-equivalent positions on the surface (for example, directly bound to an adsorbate as well as adjacent to an adsorbate-bound Pt etc.). For the qualitative identification of trends, the spectra for 4-6 atoms directly bound to O- or N-species were used because they were sufficiently different from pure metallic Pt with respect to absorption maxima positions.

Averages of the series of 4-6 spectra of Pt bound to each type of O- and N-species were further compared.

## 3. Results

### 3.1 Catalytic tests

Both studied catalysts showed a typical behavior of supported Pt in ammonia oxidation reaction (fig. 1). Their activity was similar and was shifted by 15-25 °C to lower temperatures for the more active PtA-IW-700 with bigger Pt particle size. During heating in the reaction mixture, the catalysts started to exhibit activity in $NH_3$ oxidation at 150-175 °C. PtA-IW-700 reached 50 % conversion at 209 °C ($T_{50\%}$), and PtA-IW-500 – at 224 °C. Complete conversion was observed at around 230 and 245 °C, respectively. At lower temperatures, when the conversion was not full, the catalysts demonstrated the highest selectivity to nitrogen which, for example for Pt-IW-500, decreased from the initial 65 % to 50 % at 240 °C. The rest of the products under these conditions was mainly $N_2O$, the concentration of which rose with temperature. Close to 250 °C, $N_2O$ outweighed nitrogen reaching its selectivity maximum of 55 % for PtA-IW-700 and 62 % for PtA-IW-500. With further heating, $N_2O$ selectivity gradually decreased to approx. 10 % at 400 °C. At the same time, above 240 °C $NO_x$ (NO and $NO_2$ mixture) fraction in the products started to substantially increase. For PtA-IW-700 it became the dominant product above 310 °C. PtA-IW-500 was less selective to $NO_x$, but yielded more $N_2O$. For this sample, $NO_x$ became the main product above 345 °C. In the temperature range of 240-400 °C, where $N_2O$ and $NO_x$ were prevalent, selectivity to nitrogen gradually declined from approx. 40 % to approx. 25 % for PtA-IW-700, while for PtA-IW500 $N_2$ selectivity amounted in relatively stable 25-30 % with an increase by 5-10 % above 360 °C. The catalysts showed similar trends in their performance during cooling with moderate hysteresis (fig. S3). $T_{50\%}$ decreased by 2 °C for PtA-IW-700 and by 8 °C for PtA-IW-500.

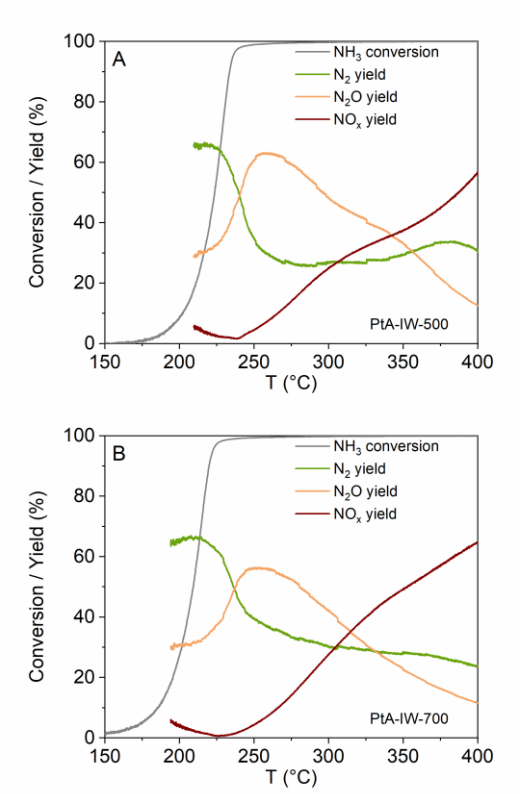


Figure 1. Catalytic activity and selectivity of A – PtA-IW-500 and B – PtA-IW-700 catalysts during the second heating in the reaction mixture (500 ppm $NH_3$ and 13 % $O_2$ in nitrogen).

3.2. Kinetic analysis

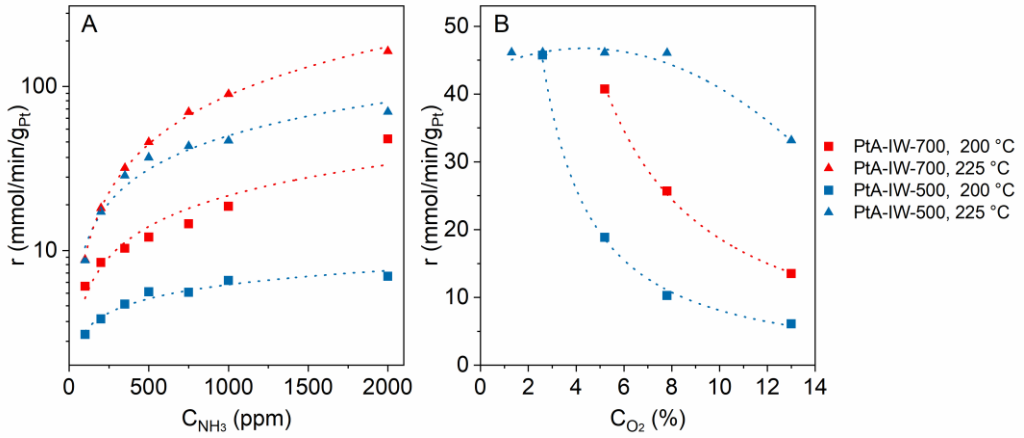


Figure 2. A – dependence of integral reaction rate on $NH_3$ concentration (constant $O_2$ concentration of 13 %); B – dependence of integral reaction rate on $O_2$ concentration (constant $NH_3$ concentration of 500 ppm). Catalysts: PtA-IW-700, PtA-IW-500.

Integral reaction rates of ammonia oxidation were determined at different concentrations of either $O_2$ or $NH_3$ in gas feed. Based on them, the apparent reaction order was estimated. For this purpose, at constant temperatures, $NH_3$ concentration was varied from 100 to 2000 ppm at unchanged $O_2$ concentration of 13 %. Similarly, $NH_3$ concentration was kept constant 500 ppm while $O_2$ concentration was altered from 1 to 13 %. Higher ammonia concentrations increased the rate of $NH_3$ conversion (fig. 2A). This points to positive reaction orders by ammonia from 0.3 to 1 (table S5). Thus, no indication of the surface poisoning by ammonia was found in the conditions studied. On the contrary, $O_2$ concentration increase leads to a drop in the reaction rate which is expressed in negative reaction orders (fig. 2B, table S5). This evidences surface poisoning by O-containing species. Hence, either high $O_2$ partial pressure or low $NH_3$:$O_2$ ratio deactivates Pt in $NH_3$ oxidation. Such deactivation trends were observed for both Pt/γ-$Al_2O_3$ catalysts with different particle sizes and at different temperatures.

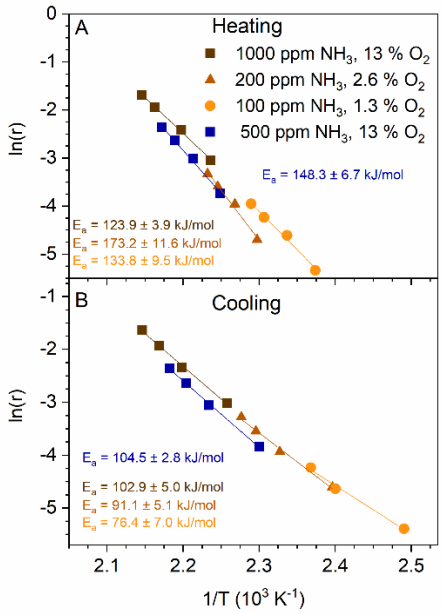


Figure 3. Arrhenius plots for $NH_3$ oxidation on PtA-IW-700 in various reaction mixtures: feeds with constant $NH_3$:$O_2$ ratio but different $O_2$ partial pressures (brown and orange lines) and feeds with different $NH_3$:$O_2$ ratios but constant $O_2$ partial pressure (lines with square markers). A – plots acquired for heating, B – plots acquired for cooling.

To determine whether it is $O_2$ partial pressure or $NH_3$:$O_2$ ratio that leads to negative reaction order, conventional light offs and light outs were carried out for PtA-IW-700 in different reaction feeds. In one case three reactant mixtures with constant $NH_3$:$O_2$ ratio but varying $O_2$ (and $NH_3$) partial pressures were tested. Ammonia concentrations were 100 ppm, 200 ppm, 1000 ppm, and oxygen concentrations – 1.3 %, 2.6 %, and 13 % respectively. In the other case, $NH_3$:$O_2$ ratio differed by 2 times while $O_2$ partial pressure remained stable. Here, a standard catalytic cycle with 500 ppm ammonia and 13 % oxygen was compared with a similar cycle where ammonia concentration was increased to 1000 ppm. The resulting catalytic data are plotted in an Arrhenius diagram (fig. 3) to calculate apparent activation energies. The plots lie fairly close to each other, which indicates that the values of apparent activation energies are in the same range. Nonetheless, they are not equal, since their slopes differ for most of the conditions. The exception are 500 and 1000 ppm of $NH_3$ with 13 % of $O_2$ during cooling (fig. 3B). The parallel lines of Arrhenius diagrams for these conditions indicate stable apparent activation energies at constant $O_2$ concentrations. At the same time, different slopes for other conditions evidence changing apparent activation energies with the change of $O_2$ content in the reaction mixture, in line with the previous conclusions.

The change of the apparent activation energy in different reaction feeds is visualized in fig. 4. During heating the $E_a$ did not show any clear trend with respect to $O_2$ partial pressures. However, the $E_a$ values were relatively high exceeding those obtained during the cooling 1.2-1.9 times. On the other hand, a trend in apparent activation energy change during cooling was seen. Variation of $NH_3$:$O_2$ ratio while keeping the same $O_2$ partial pressure (reaction feeds with 500 and 1000 ppm $NH_3$ and 13 % $O_2$) did not alter $E_a$. At the same time, the change of $O_2$ partial pressures clearly affected $E_a$ during the cooling. Apparent activation energy substantially increased with rising oxygen concentration. A relatively high $E_a$ values during heating and their increase with raising $O_2$ partial pressure during cooling may be an indication of the dependence of apparent activation energy on surface oxygen coverage and a high adsorption energy of oxygen. Thus, the relatively high equilibrium constant of O adsorption contributes to the elevated apparent $E_a$ values during heating. During cooling, when much of oxygen

is desorbed, a direct correlation of $E_a$ with $O_2$ concentration, hence with its surface coverage, is observed. These results suggest that high oxygen coverage on platinum surface makes this metal inactive in ammonia oxidation. During light off, surface oxygen desorbs with rising temperature leaving the surface clean and available for ammonia oxidation.

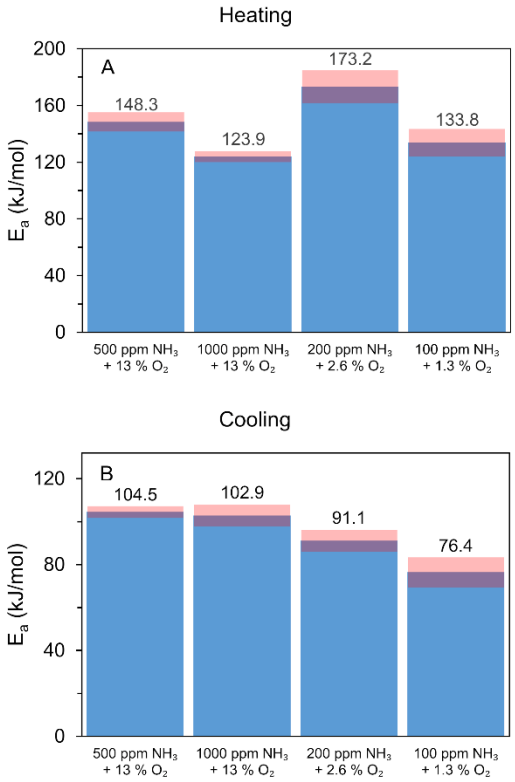


Figure 4. Change of apparent activation energies for PtA-IW-700 in various reaction mixtures: feeds with constant $NH_3$:$O_2$ ratio but different $O_2$ partial pressures and feeds with different $NH_3$:$O_2$ ratios but constant $O_2$ partial pressure; A – acquired for heating, B – acquired for cooling.

It is interesting to compare these trends of changing apparent activation energies on the opposite sides of hysteresis with those of other oxidation reactions typical for emission control. For example, in the case of CO oxidation over Pt particles in a similar size range as in this work (larger than about 2 nm) which is common in industrial applications, lower activity during heating is caused by CO poisoning. During cooling Pt is oxidized and exhibits higher activity.[67, 68] This is in line with a report of apparent activation energy of CO oxidation increasing from 75 kJ/mol over platinum oxide to 93 kJ/mol over

reduced and CO-poisoned Pt.[69] Although measured under ultrahigh vacuum, these results are consistent with those obtained under atmospheric pressure.[70] Notably, for CO oxidation, even the less active poisoned Pt during ignition leads to lower or similar apparent $E_a$ as the more active Pt state during $NH_3$ oxidation extinction (for $O_2$ concentrations > 1.3 %, cf. fig. 4). In agreement with this, CO oxidation over Pt generally occurs at lower temperatures than ammonia oxidation under analogous conditions. Contrary to CO, the oxidized and reduced states of Pt surface play a different role in hysteresis during methane oxidation. In this case, the reaction is faster over reduced Pt.[71] Specifically, ignition starts when oxygen is at least partially removed from platinum surface.[71, 72] As a result, a more active reduced state persists at lower temperatures during cooling causing hysteresis.[71, 72] Apparent activation energies over reduced Pt for lean $CH_4$-air mixtures (equivalence ratios 0.3-0.5) are reported to be to 66-88 kJ/mol.[72, 73] These are lower than during cooling in ammonia oxidation (fig. 4) where lower fuel-to-oxygen ratios were used. The authors also discussed the increase of apparent $E_a$ at higher $O_2$ concentrations, like in the case of ammonia oxidation.[73] Concerning the light-off, the apparent activation energy of methane oxidation was significantly higher and amounted to 166-188 kJ/mol for the same abovementioned $CH_4$-air mixtures.[73] The authors connected this increase with the apparent activation energy required for oxygen desorption in presence of methane. The reported apparent activation energies during methane oxidation ignition are similar to the highest values that are observed for ammonia oxidation in fig. 4. This hints that lower activity during heating in $NH_3$ oxidation feed may be caused by the same step of $O_2$ desorption which has a considerably high activation energy.

### 3.3. *Operando* DRIFTS studies

To determine the nature of the adsorbed surface species and their influence on the catalyst performance *operando* DRIFTS spectra were acquired on the PtA-IW-700 catalyst in the reaction feed (500 ppm $NH_3$, 10% $O_2$ in He) at 100-400 °C. The spectra recorded at constant temperatures when reaching steady states are presented in fig. 5 together with simultaneously recorded catalytic data.

General trends in the catalytic data obtained during DRIFTS measurements were similar to the results from the conventional laboratory reactor (fig. 5A). Ammonia oxidation light-off took place between 150 and 200 °C reaching conversions close to complete at higher temperatures. In the low temperature range, from the conversion start to reaching approximately complete conversions (150-

200 °C), the selectivity to nitrogen was predominant. At 200 °C, in the point of the highest $N_2$ yield, significant amounts of $N_2O$ were also detected. With further temperature raise above 350 °C NO became the predominant product. Practically no $NO_2$ was detected among the products during the tests in the DRIFTS cell.

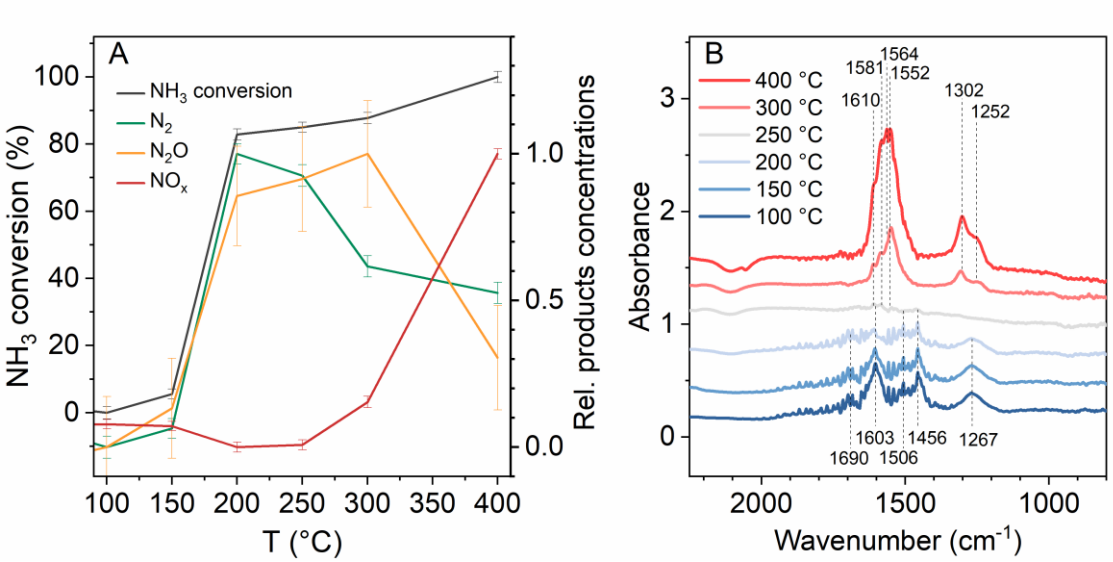


Figure 5. Results of *operando* DRIFTS measurements for PtA-IW-700: A – catalytic data, products determined by a mass spectrometer; B – DRIFTS spectra recorded at different temperatures. Reaction mixture – 500 ppm $NH_3$, 10 % $O_2$ in He, flow – 100 $cm^3$/min. 60 mg of the catalyst.

Simultaneously recorded DRIFTS spectra could be described with adsorption bands of two major surface species: either ammonia-derived adsorbates or nitrate-groups (fig. 5B). The first group of bands originating from ammonia-derived species was mainly present at lower temperatures. It included the bands at 1692 and 1509 $cm^{-1}$ corresponding to $NH_3$ on Brønsted acid sites.[35] In turn, the band at 1267 $cm^{-1}$ can be attributed to $NH_3$ on Lewis acid sites.[35] The other absorption band most likely belongs to ammonia dissociation products: scissorings of $NH_2$ group at 1603 $cm^{-1}$ and deformation of NH group at 1456 $cm^{-1}$.[35, 74] The second group of bands corresponding to nitrates that evolved at high temperatures. The bands at 1564 – 1552 $cm^{-1}$ and 1252 $cm^{-1}$ originate from the asymmetric and symmetric stretch of monodentate $NO_2$ group, respectively.[75] A broad band around 1252 $cm^{-1}$ most likely contains additional

less intense features of two types of bidentate species – bridging nitrate (about 1210 $cm^{-1}$) and bridging nitrite (about 1230 $cm^{-1}$).[75] Although it is difficult to distinguish each of them in this region, other characteristic bands of bridging nitrates and bridging nitrites are present: at 1610 $cm^{-1}$ at 1302 $cm^{-1}$, respectively.[75] The feature at 1302 $cm^{-1}$ may also belong to an asymmetric stretch of chelating bidentate nitrate.[75] A symmetric stretch for this group locates at 1581 $cm^{-1}$.[75] Although it is difficult to unambiguously attribute all the spectral features observed at high temperatures, they exhibit a typical profile of $NO_x$ interacting with alumina support and consisting mainly of nitrates.[75]

The evolution of the spectral profile correlated with the change of catalytic activity and selectivity. For instance, at low temperatures, where nitrogen selectivity was the highest, the spectra showed abundant presence of ammonia on the catalyst surface that decreased with heating. At 250 °C, when nitrogen selectivity started to decline, $N_2O$ became the main product. At this point, a relatively clean catalyst surface with hardly detectable absorption bands of ammonia or nitrates was observed. This observation is consistent with the results reported in refs. [31, 36] where $N_2O$ selectivity increased in the lack of adsorbed ammonia on Pt surface. Starting from 300 °C, pronounced absorption bands of nitrates began to rise in the spectra. This was accompanied with the buildup of selectivity to NO. Despite the clear correlation between the detection of nitrates and NO selectivity, it is hard to tell whether nitrates are the source of $NO_x$ in the products or the result of $NO_x$ reaction with the support. In case of titania-supported Pt described in ref. [36], no surface $NO_x$ or nitrates were detected while $NO_x$ yield was still high. This suggests that nitrates are rather the products of $NO_x$ reaction with $Al_2O_3$ support. In turn, $TiO_2$ may not form nitrates because of its lower basicity compared to alumina.

*Operando* DRIFTS has shown an important role of the support in selectivity to nitrogen. This can be better understood in the light of the studies conducted under model conditions.[76-78] They reported that NO can be produced only when all adsorbed $NH_x$ (x=1-3) species are dehydrogenated. This is fairly close to the observation made in the current study under atmospheric pressure. Specifically, $NO_x$ started to evolve to a considerable extent only when the catalyst surface was deprived of the adsorbed $NH_x$ species. At the same time, $N_2O$ was the product in the transition between the predominant $N_2$

yield in the excess of $NH_x$ and the relatively clean surface where $NO_x$ started to evolve. Nitrous oxide is not commonly reported in the model studies conducted under vacuum, therefore the current experiment complements them with the data acquired under the atmospheric pressure.

Despite these results are generally consistent with the results of other methods and previous publications, *operando* DRIFTS has no possibility to distinguish between surface species on Pt and the support. For this reason, to conclude about the specific species on Pt one needs to apply complementary element-specific spectroscopic methods like *operando* XAS.

### 3.4. *Operando* XAS studies

#### 3.4.1. Heating in the reaction mixture

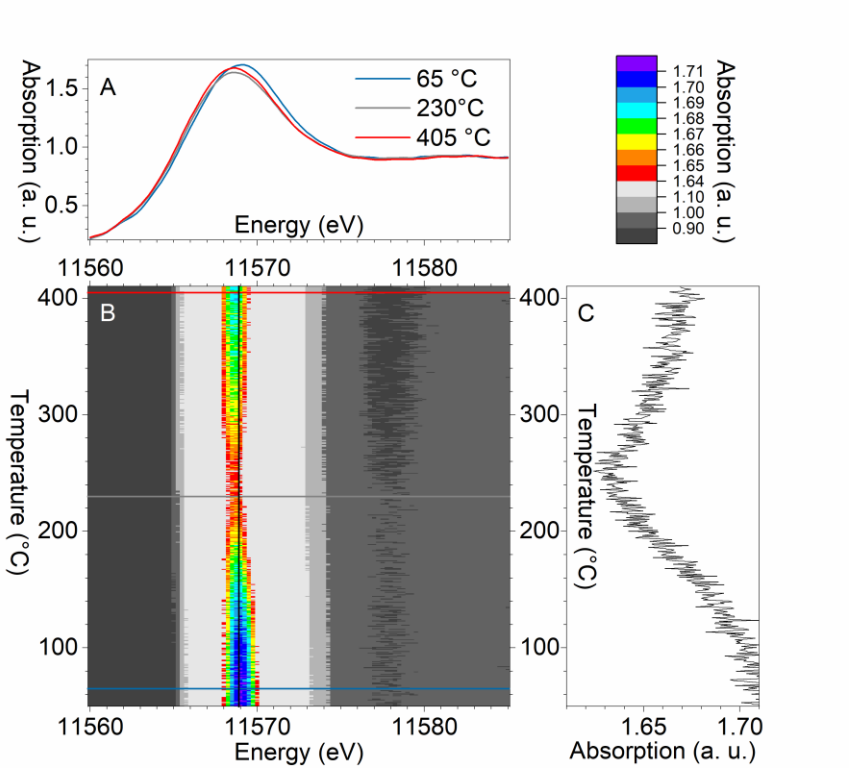


Figure 6. Contour plot for Pt $L_3$ normalized *operando* XANES spectra of PtA-IW-500 recorded during the second heating in the reaction mixture (500 ppm $NH_3$ and 10 % $O_2$, inert balance). A – energy profiles of the contour plot at three different temperatures that corresponded to the spectra with the most different shapes (see a comparison with Pt and $PtO_2$ references in figure 4A). B – the contour plot. C – X-ray absorption profile at the energy near the maximum absorption intensity (11568.9 eV).

In order to identify species adsorbed on Pt surface at different temperatures we performed temperature-programmed reaction on both $Pt/Al_2O_3$ samples in $NH_3$ oxidation gas mixture (500 ppm $NH_3$ and 10 % $O_2$ in He) while simultaneously recording QEXAFS spectra.

The QEXAFS spectra recorded for the PtA-IW-500 sample during heating in the reaction mixture are presented as a contour plot in fig. 6. The absorption intensity in this case is presented through the color map. On the contour plot, *y*-axis projection is a spectrum at a certain temperature (fig. 6A), and *x*-axis projection – normalized absorbance at a certain energy (fig 6C). In our case, the *x*-axis projection was selected near the absorption maximum – at 11568.9 eV. As it can be seen from this projection, the maximum intensity decreased during heating in the reaction mixture and reached its minimum at 230 – 260 °C. With further temperature increase, the absorbance grew again. The intensity of the Pt $L_3$ absorption maximum correlates with the electron density.[79] The intensity drop is a sign of Pt reduction, while higher intensity points to its oxidation. Therefore, it can be concluded that Pt became more reduced during the light off in the reaction mixture at 230 – 260 °C and afterwards re-oxidized at higher temperatures.

A closer look at the temperature profiles of the contour plot at low temperature, at the temperature of absorption minimum and at high temperature revealed three distinct spectral shapes in the region around the absorption edge (this region is also known as a “white line”). These spectra differed not only in their intensity, but also in the energies corresponding to absorption maxima. During heating in the reaction mixture, the white line maximum shifted to lower energy values. This indicates a change in coordination environment of Pt and suggests that the two oxidized states at high and low temperatures are not equivalent.

Catalytic data obtained in parallel to QEXAFS measurements are presented in fig. 7A. The light off started at 170 °C. With further heating, $T_{50\%}$ was reached at 215 °C and full conversion at 260 °C. The qualitative trends in catalyst selectivity were similar to those observed in a laboratory setup. For example, the highest nitrogen yield emerged after the start of the light off and retained until the temperature of full conversion. Then selectivity to $N_2$ decreased in favor of $N_2O$ which had its

production maximum at 280 °C with subsequent decline. In parallel, after reaching complete conversion, $NO_x$ started to evolve, gradually increasing their yield till 400 °C.

To gain a deeper insight, the measured QEXAFS data were further analyzed using the multivariate curve resolution (MCR) algorithm. In this way, three spectral components were identified that are shown in fig. 7B. In general, these spectra were very similar and located in between Pt foil and $PtO_2$ reference spectra suggesting partially oxidized state of Pt (fig. S4). The moderate differences between the spectra implied that they corresponded to three states of Pt nanoparticles which had most of their bulk atoms unchanged and differed mainly with their surface sites. The MCR-derived spectral components were then used as references to conduct linear combination analysis (LCA) of the measured spectra. In this way, we could estimate the contribution of each component in the *operando* spectra and thus follow the change of Pt phase composition. The relative fraction of each component in the spectra measured at certain temperature is plotted in fig. 7C.

The first of the three spectral components (blue lines in fig. 7B, C) was the most abundant at low temperatures (inactive catalyst state). It had the highest white line intensity implying the most oxidized Pt state compared to the other two.[79] As soon as the fraction of the low-temperature component fell below 40 % around 170 °C, light off started. At this point, the second spectral component became predominant (marked with the grey line in fig. 7B, C).

Compared to the low temperature component, the white line of the second spectral component (marked in grey in fig. 7B, C) slightly shifted to lower energies and was less intense indicating Pt reduction.[79] Along with the build-up of the second component, ammonia conversion also increased and became 100 % at approx. 250-260 °C. This aligned with the maximum concentration (approx. 55 %) of the second component. The upturn of this more reduced Pt phase correlated with the highest selectivity to nitrogen.

After the onset of full conversion at temperatures over 260 °C, the third spectral component started to prevail (marked in red in fig. 7B, C). Its higher absorption maximum, compared to the second component, pointed to re-oxidation of platinum. The white line also shifted to lower energies, which

implied the change in coordination environment of Pt. In this case, the yield of $N_2O$ exceeded that of $N_2$ with a maximum at 280 °C and then gradually decreased. At the same time, selectivity to undesirable $NO_x$ grew monotonously from 0 to approx. 20 % in the whole temperature interval where the high temperature spectral component was prevailing.

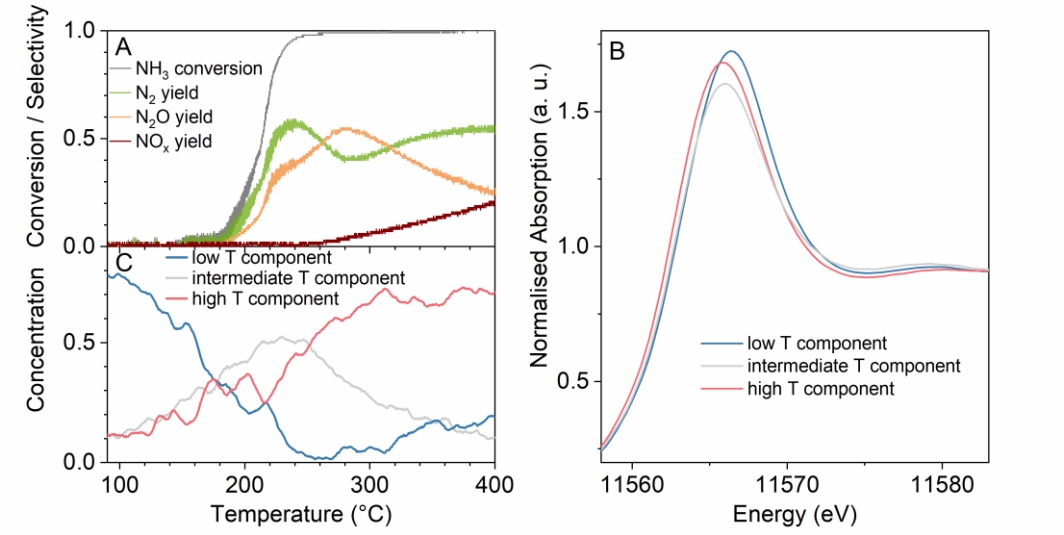


Figure 7. Results of *operando* QEXAFS measurements for PtA-IW-500 during the second heating in the reaction mixture (500 ppm $NH_3$ and 10 % $O_2$, inert balance): A – catalytic data; B – the most distinct spectral components derived by MCR; C – contribution of the three most distinct spectral components to the experimental spectra. Maximum concentrations for spectral components were observed at the following temperatures: low-temperature component – below 100 °C; intermediate-temperature component – about 230 °C; high-temperature component – above 310 °C.

The abovementioned spectral behavior and its correlation with catalytic activity and selectivity was observed not only for the PtA-IW-500 sample. In particular, a similar QEXAFS experiment conducted for PtA-IW-700 with less dispersed Pt revealed the same trends as those reported above (figs. S5 and S6). The difference from PtA-IW-500 with smaller nanoparticles was that the changes in the phase content of PtA-IW-700 were less pronounced yet clearly noticeable. This can be explained with the lower contribution of the surface atoms participating in the reaction because of the

significantly larger Pt particle diameter and the bulk averaging nature of XAS. Moreover, we previously reported analogous observations of three spectral components with Pt reduction and re-oxidation for Pt on zeolite.[50] In general, for alumina- and zeolite-supported Pt particles larger than approx. 2 nm, the oxidized low-temperature component corresponded to the inactive state, the more reduced intermediate-temperature component was linked to high activity and selectivity, and another oxidized component associated with low selectivity yet high activity at elevated temperatures. Such a similar spectral trend in connection with catalytic performance proved a common reaction mechanism. Therefore, the variation of the Pt surface state reflected in the observed spectra seems to be the key to a better understanding of $NH_3$ oxidation mechanism.

Hence, the identification of the species at the origin of the observed spectral features is required to reveal Pt surface structures responsible for its catalytic activity and selectivity. In this respect, the oxidized Pt state at low temperatures corresponds to inactive Pt, probably, due to O-containing poisoning species as evidenced from the kinetic studies. In turn, the other two spectral components are more difficult to determine based on the data discussed above. *Operando* DRIFTS results only indirectly hint that the intermediate temperature component could correspond to more reduced Pt covered with ammonia-derived species. Furthermore, the identification of the high-temperature component is even less clear. The XAS results suggest that it is oxidized however not equivalent to the low-temperature component, based upon its white line shift.

### 3.4.2. Treatment in model atmospheres

To further identify the Pt surface states discovered during $NH_3$ oxidation we performed temperature-programmed heating of PtA-IW-500 with individual educts / products while simultaneously measuring QEXAFS spectra. The atmospheres in which the sample was treated were pure He, 500 ppm $NH_3$, 10 % $O_2$, 500 ppm NO, a mixture of 500 ppm NO and 10 % $O_2$.

The contour plots obtained from the spectra recorded in different atmospheres are presented in figs. S7-S11. First, the sample was heated in He. In this atmosphere, Pt was reduced with the decrease

of a white line intensity comparable to the heating in the reaction mixture – to 1.6-1.7 (cf. figs. S7 and 6). However, in contrast to the heating in the reaction mixture, the sample did not re-oxidize at high temperatures even though the red shift of the white line was still present.

During heating in $NH_3$, the sample underwent strong reduction with much higher intensity decrease than observed in the reaction mixture (fig. S8). This was followed by subsequent treatments of the catalyst in diluted NO, NO and $O_2$ mixture, and $O_2$. All these atmospheres led to surface oxidation of Pt (figs. S9-S11). The final average oxidation state was higher in the oxygen-containing media. The analysis of the gas mixture composition at the reactor outlet during the treatment in NO atmosphere has shown both products of NO disproportionation – $N_2O$ and $NO_2$ (fig. S12B). The nitrogen mass balance corresponded to the conversion of NO in the feed. However, $N_2O$ concentration exceeded $NO_2$ concentration almost twice, which suggests probable oxygen deposition on Pt resulting in its oxidation.

Similarly to the analysis of the results obtained in the reaction mixture, spectral components were extracted for measurements in model gas mixtures. For this purpose, prior to the MCR algorithm discussed above, the *SIMPLISMA* algorithm was applied.

The most distinct spectral components recorded in He atmosphere (Fig. 8) were similar to the ones obtained in the reaction feed. This was the case for both MCR and *SIMPLISMA* analyses (cf. fig. 8 and fig. S13A, B). As discussed before, after the start of heating in He Pt was reduced (cf. blue and grey lines in fig. 8A). With the further temperature increase, the spectra shifted to lower energies, like in the reaction feed, but without an increase in the white line intensity (cf. grey and red lines in fig. 8A). Thus, despite being similar to the spectral components in the reaction mixture, the spectra in He had small energy shifts and slightly lower intensities (see fig. 8B, C). This indicates less pronounced changes of the Pt surface species compared to the reaction mixture.

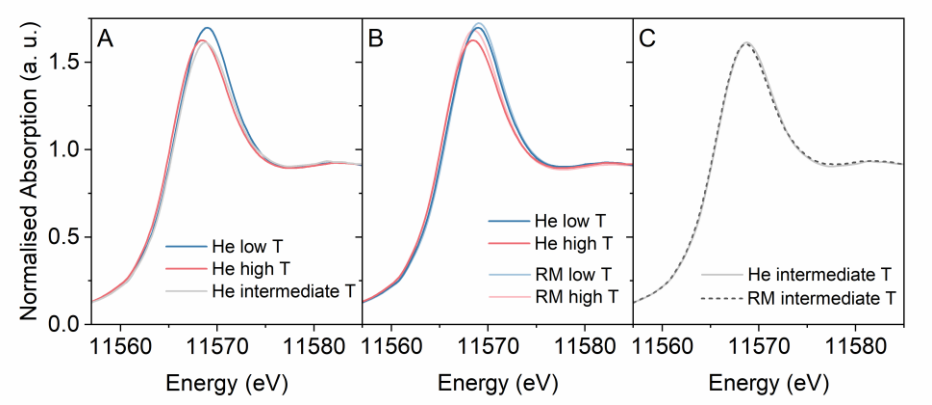


Figure 8. The MCR-derived most distinct spectral components for the Pt $L_3$ XANES spectra of PtA-IW-500: A – in He atmosphere; B – in He atmosphere compared to the ones dominating in the reaction mixture (RM) at high and low temperatures; C – in He atmosphere compared to the one dominating in the reaction mixture at intermediate temperature. Maximum concentrations for spectral components in He were observed at the following temperatures: low-temperature component – 50 °C; intermediate-temperature component – about 220 °C; high-temperature component – 400 °C (see fig. 7 for the temperatures of the components in the reaction mixture).

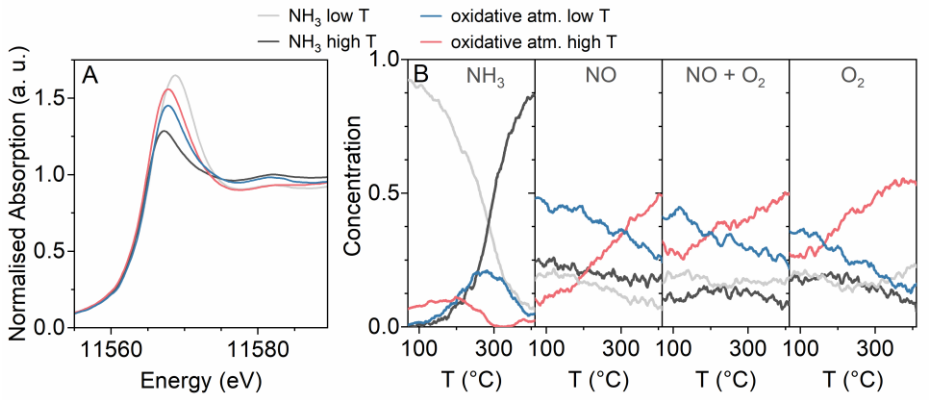


Figure 9. A – MCR-derived most distinct spectral components for the Pt $L_3$ XANES spectra recorded during heating of PtA-IW-500 in reductive ($NH_3$) and oxidative (NO, $O_2$, and their mixture) atmospheres. B – contributions of the four most distinct MCR-derived spectral shapes to the experimental spectra during heating in reductive and oxidative atmospheres. For the spectral components in all atmospheres presented in the figure, low temperature and high temperature correspond to 50 and 400 °C, respectively.

The spectral data collected in four following atmospheres – $NH_3$, pure NO, $O_2$ and their mixture – were analyzed with the MCR and *SIMPLISMA* algorithms as one batch in order to search for common spectral components. In this way, four components were found by both methods and are shown in figs. 9, S14 and S15. Similar trends were uncovered by both algorithms, namely, two spectral components dominated in the reductive environment of $NH_3$ (light grey and dark grey lines in fig. 9) and the other two – in all remaining oxidizing environments (red and blue lines in fig. 9). These spectral shapes were then compared with the ones acquired under reaction conditions to obtain a better understanding of the nature of the surface species governing Pt activity and selectivity (figs. S16, S17).

Of the two dominant components found for Pt in $NH_3$ atmosphere, one was very similar to the intermediate-temperature component observed during the light off in the reaction mixture. These spectra are compared in fig. S16. In the case of MCR analysis the two spectra had the same maximum absorption energy hinting to the same coordination environment of Pt. At the same time, the white line intensity in $NH_3$ was slightly higher, which could imply different surface concentration of the same adsorbate. *SIMPLISMA* analysis resulted in practically identical spectral components for $NH_3$ atmosphere at low temperatures and the spectral component in the reaction mixture at intermediate temperatures, during the light off (fig. S13C). This implied that the intermediate temperature state of platinum, responsible for high activity and selectivity to $N_2$, was probably Pt with adsorbed $NH_3$ / $NH_x$ species.

With the further heating in ammonia, Pt species strongly reduced and could not be oxidized to the initial state during the following oxidative treatments (fig. S17). The sign of this was the strong decrease in the absorption intensity (black curve) that did not recover in oxidative environments (the spectra in red and blue). Hence, at that point it was not possible to directly compare Pt states with those obtained in the reaction mixture. However, the presence of only two main spectral components for all three oxidative atmospheres (containing NO and not containing it) meant that the species at the origin of these spectra did not contain nitrogen atoms. Thus, the low-temperature and the high-

temperature components under reaction conditions may both contain exclusively oxygen atoms with different types of binding to Pt or in different surface or interstitial locations.

To better understand the spectral features observed by *operando* XAS in this study, it is helpful to analyze the reports of surface species in ammonia oxidation described in literature. This analysis is based on works [14, 17, 19-21, 23, 24, 33, 34, 36, 38, 80-93] and presented in detail on pp. S12-S14 of the SI. In short, two most frequently reported groups of species existing on Pt under reaction conditions are either ammonia- or oxygen-based. The first group includes $NH_3$ and its dissociation products $NH_x$ (x = 0-2). The second group is represented by oxygen in oxidic or atomically adsorbed form as well as oxygen in subsurface layers of metallic Pt. Since measuring XAS references of many of the above-mentioned species would pose significant difficulties, DFT modelling was used to obtain the most energetically favourable geometries of the reaction-relevant educts in surface Pt layers. These geometries were further employed to calculate the corresponding Pt $L_3$ XANES spectra.

### 3.5 Modelling trends in XANES spectral shapes

Pt $L_3$ spectra with different adsorbates on Pt(100) surface were modelled to confirm the assignment of the spectral components observed during $NH_3$ oxidation. The initial geometries for modelling the most energetically favourable positions of $NH_3$ / $NH_x$ species on Pt(100) surface ($NH_3$ atop, $NH_2$ bridge, NH hollow, and N hollow positions) were taken from ref. [80]. The initial geometries for modelling O in the hollow position on the Pt surface and in tetrahedral position in its subsurface were based on ref. [92]. The optimised structures used for spectra calculation are illustrated in fig. S18. The *xyz*-coordinates of their atoms can be found in ref. [64]. The resulting absorption edge position and intensity in the spectra calculated from these models cannot be directly compared to the experimental ones due to large errors in absolute energy scale calculations and potentially different energy resolution. Therefore, distance between the first and the second most intense absorption maxima and the high energy side slope of the most intense absorption band (white line, figs. 10, S19) were chosen to follow the trends in the spectral shape for the modelled structures.

For better comparison of slope steepness and distance between the first and the second absorption maxima, all experimental and theoretical spectra were aligned to the same energy position of the highest absorption intensity (i.e. white line).

The trends observed in the modelled spectra allow to attribute the spectra observed at low and intermediate temperatures in the reaction mixture. As it is demonstrated in fig. 10C, the second most intense absorption band in the experimental spectra is located in the same range for both the low-temperature and the intermediate-temperature components (blue and grey curves). This range was also common for calculated spectra with surface O and $NH_x$ species adsorbed on Pt. However, the calculated spectra of these species differed in the white line slope steepness. For all N-containing species the slope was much shallower than for O-covered surfaces. The spectrum with the least pronounced shallow slope among the N-containing species is compared to the least steep slope among the O-containing species in fig. S19. At the same time, distinct trends in slope steepness could be seen among the experimental spectra from fig. 10C. For the low-temperature component and the high-temperature component, the slope was clearly steeper than for the intermediate-temperature component observed during the light-off. Therefore, the modelled spectra confirmed that the low-temperature spectral component is related mainly to Pt with surface O, in line with the previous assumptions. In turn, the intermediate-temperature component from the experimental spectra rather resembled the spectrum of Pt with adsorbed $NH_3$ / $NH_x$. The calculated spectrum of pure Pt(100) surface did not match the spectrum of the intermediate-temperature component well because of a steeper slope and lower distance between the two most intense bands. This supported the attribution of the middle-temperature component from the reaction mixture rather to $NH_3$ / $NH_x$ species than to clean Pt surface, despite the apparent similarity of the experimental spectra in He and in $NH_3$ noted in section 3.4.2.

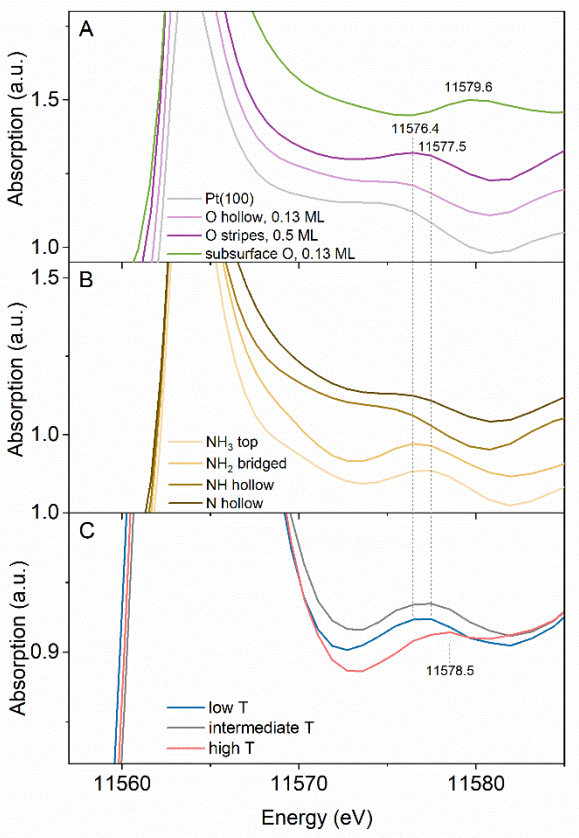


Figure 10. Comparison of the experimental *operando* XANES spectra of PtA-IW-500 obtained during heating in the reaction mixture (500 ppm $NH_3$ and 10 % $O_2$, inert balance) with the modelled XANES spectra of Pt with different adsorbates: A – calculated spectra of surface Pt(100) atoms on pure Pt cluster and modelled spectra of Pt in the same cluster contacting with O species; B – modelled spectra of surface Pt(100) atoms contacting with adsorbed $NH_3$ or its dissociation products; C – experimental spectra. Maximum concentrations for spectral components in the reaction mixture were observed at the following temperatures: low-temperature component – below 100 °C; intermediate-temperature component – about 230 °C; high-temperature component – above 310 °C.

Spectral modelling was also used to identify the high-temperature component from the experimental data in the reaction mixture. A clear trend of increasing distance between the two most intense absorption bands was observed with rising temperature (fig. 10C). A shift in the same direction is observed upon formation of Pt with subsurface O. It has the second absorption maximum at higher energy than surface O with the same coverage (fig. 10A). Nonetheless, the position of the second band

in the calculated spectrum did not precisely match the second band for the experimental spectrum. This may be explained with simultaneous presence of multiple types of adsorbates on Pt. The surface may still contain some O which was not reduced during the light off. Moreover, higher surface coverage with O species stabilizes subsurface O structures.[93] This increases the likeliness of the co-existence of surface and subsurface oxygen. Hence, the features of both species would be observed in the experimental spectrum. For example, fig. S20 shows the spectra of surface and subsurface O after averaging. On the averaged spectrum the second absorption maximum moves closer to the first one and approaches the one observed experimentally at high temperature.

**4. Conclusions**

In this work the main states of Pt that govern its activity and selectivity in ammonia oxidation on $Pt/Al_2O_3$ were studied. To identify these states, kinetic analysis, *operando* DRIFTS and XAS, and XANES spectral modelling were applied. Kinetic analysis showed that a high coverage by O-containing species poisoned Pt surface at low temperature At the same time, ammonia did not deactivate the catalyst under the conditions tested (up to 1000 ppm concentration). This was further confirmed with *operando* DRIFTS analysis which showed abundance of $NH_3$ on the catalyst at low temperature which remained during the light off until the full conversion was reached. This was followed by the decline of adsorbed ammonia and the growth of $N_2O$ and $NO_x$ yield. Furthermore, the *operando* XAS and modelling studies revealed three main states of platinum during ammonia oxidation with the spectra shown in fig. 11B. The species observed at low temperatures contained oxygen that poisoned Pt surface and made it inactive in ammonia oxidation (see fig. 11A, D). With temperature increase this O-containing species decomposed or desorbed enabling $NH_3$ dissociation, which gave rise to $NH_x$ species. In this state the Pt surface started to be active with high selectivity to the desired product nitrogen (cf. fig. 11A, D). At higher temperature, due to fast conversion, the coverage of ammonia and $NH_x$-species on the surface was low. This made it prone to oxidation by reaction with another type of O-species. Most likely, under the influence of high temperature and high surface O coverage, some oxygen atoms

diffused into subsurface of Pt crystal lattice (fig. 11 D). This state did not prevent high activity. However, it was associated with selectivity to the undesired reaction products $N_2O$ and NO due to the low coverage of $NH_x$ species and higher probability for them to interact with surface oxygen than with other N-containing moieties under these conditions. Surface oxygen desorption during heating in the reaction mixture was also likely to be the reason of significantly higher apparent activation energies during the light-offs compared to the light-outs. This led to hysteresis when the catalysts were more active during cooling with subsurface O and $NH_x$-covered surface persisting at lower temperatures in the absence of fully O-covered Pt.

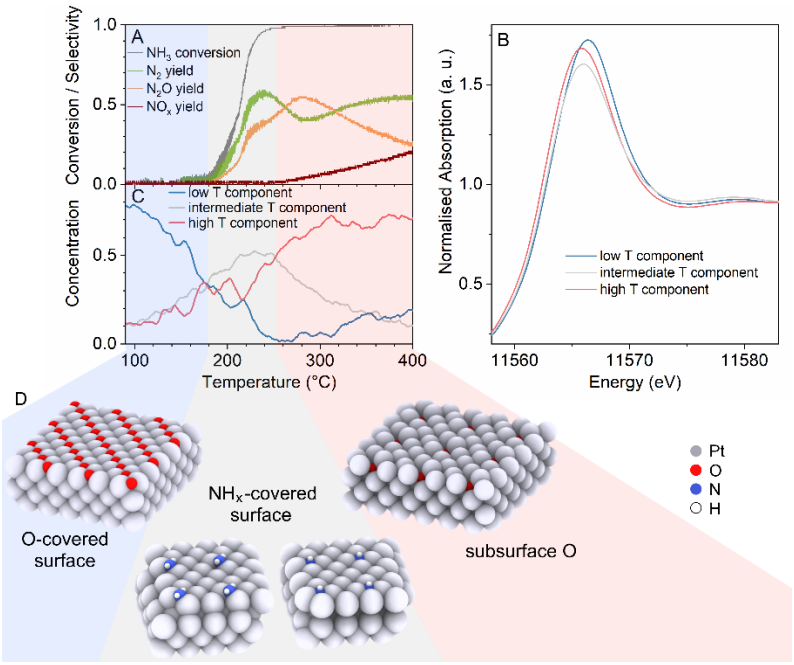


Figure 11. Surface and subsurface species in the top Pt layers at the origin of a typical spectral trend for Pt under reaction conditions, which prevail in different modes of Pt activity and selectivity. The experimental data obtained for *operando* QEXAFS measurements of PtA-IW-500 during the second heating in the reaction mixture (500 ppm $NH_3$ and 10 % $O_2$, inert balance): A – catalytic results; B – the most distinct spectral components derived by MCR; C – contribution of the three most distinct spectral components to the experimental spectra; D – species in surface and subsurface structures of Pt deferring at the various temperature regimes of the light off.

**Supporting information**. Weisz-Prater parameters estimation, activity comparison in the first and the second catalytic cycles, mass spectrometry results quantification, catalytic activity and selectivity during the second cooling , comparison of the experimental and the MCR-derived *operando* XAS spectra for PtA-IW-500 with Pt and $PtO_2$ references, *operando* XAS data for PtA-IW-700, additional results on catalyst treatment in oxidative and reductive atmospheres, overview of species in surface layers of platinum under reaction conditions, additional results of XANES spectra calculations

**Acknowledgement.** This study was funded by the Initiative and Networking Fund of the Helmholtz Association, grant HRSF-0046.

DESY (Hamburg, Germany), a member of the Helmholtz Association HGF, is acknowledged for the provided beamtime I-20200270 at PETRA III. The authors are grateful to Dr. Wolfgang Caliebe and Dr. Vadim Murzin for their assistance in using beamline P64.

The authors would also like to thank Dr. Paolo Dolcet and Simon Barth (ITCP and IKFT respectively, KIT) for their help during synchrotron measurements, Dr. Andrey I. Stadnichenko, Dr. Lidiya S. Kibis, Dr. Dmitry A. Svintsitskiy, and Prof. Dr. Andrei I. Boronin (Boreskov Institute of Catalysis, Novosibirsk) for insightful discussions and project planning. We further thank Dr. Ton V.W. Janssens (Umicore Denmark) for fruitful discussions.

The authors acknowledge support by the state of Baden-Württemberg through bwHPC and the Deutsche Forschungsgemeinschaft (DFG, German Research Foundation) through grant no. INST 40/575-1 FUGG (JUSTUS 2 cluster, RVs bw17D011). Finally, the authors acknowledge the Deutsche Forschungsgemeinschaft (DFG, German Research Foundation) for funding within the Collaborative Research Center 1441 “Tracking the Active Site in Heterogeneous Catalysis for Emission Control (TrackAct)” (Project-ID 426888090).

**References**

(1) Valera-Medina, A.; Xiao, H.; Owen-Jones, M.; David, W. I. F.; Bowen, P. J. Ammonia for power. *Prog. Energy Combust. Sci.* **2018**, *69*, 63-102.

(2) Kojima, Y. Hydrogen storage materials for hydrogen and energy carriers. *Int. J. Hydrog. Energy* **2019**, *44* (33), 18179-18192.
(3) Miura, D.; Tezuka, T. A comparative study of ammonia energy systems as a future energy carrier, with particular reference to vehicle use in Japan. *Energy* **2014**, *68*, 428-436.
(4) Giddey, S.; Badwal, S. P. S.; Munnings, C.; Dolan, M. Ammonia as a Renewable Energy Transportation Media. *ACS Sustain. Chem. Eng.* **2017**, *5* (11), 10231-10239.
(5) Morlanes, N.; Katikaneni, S. P.; Paglieri, S. N.; Harale, A.; Solami, B.; Sarathy, S. M.; Gascon, J. A technological roadmap to the ammonia energy economy: Current state and missing technologies. *Chem. Eng. J.* **2021**, *408* (15), 127310.
(6) Gao, F.; Liu, Y.; Sani, Z.; Tang, X.; Yi, H.; Zhao, S.; Yu, Q.; Zhou, Y. Advances in selective catalytic oxidation of ammonia ($NH_3$–SCO) to dinitrogen in excess oxygen: A review on typical catalysts, catalytic performances and reaction mechanisms. *J. Environ. Chem. Eng.* **2021**, *9* (1), 104575.
(7) Lan, T.; Zhao, Y.; Deng, J.; Zhang, J.; Shi, L.; Zhang, D. Selective catalytic oxidation of $NH_3$ over noble metal-based catalysts: state of the art and future prospects. *Catal. Sci. Technol.* **2020**, *10* (17), 5792-5810.
(8) Dhillon, P. S.; Harold, M. P.; Wang, D.; Kumar, A.; Joshi, S. Hydrothermal aging of $Pt/Al_2O_3$ monolith: Washcoat morphology degradation effects studied using ammonia and propylene oxidation. *Catal. Today* **2019**, *320*, 20-29.
(9) Chmielarz, L.; Jabłońska, M. Advances in selective catalytic oxidation of ammonia to dinitrogen: a review. *RSC Adv.* **2015**, *5* (54), 43408-43431.
(10) Scheuer, A.; Votsmeier, M.; Schuler, A.; Gieshoff, J.; Drochner, A.; Vogel, H. $NH_3$-slip catalysts: Experiments versus mechanistic modelling. *Top. Catal.* **2009**, *52* (13-20), 1847-1851.
(11) Colombo, M.; Nova, I.; Tronconi, E. Detailed kinetic modeling of the $NH_3$–$NO/NO_2$ SCR reactions over a commercial Cu-zeolite catalyst for Diesel exhausts after treatment. *Catal. Today* **2012**, *197* (1), 243-255.
(12) Scheuer, A.; Hauptmann, W.; Drochner, A.; Gieshoff, J.; Vogel, H.; Votsmeier, M. Dual layer automotive ammonia oxidation catalysts: Experiments and computer simulation. *Appl. Catal. B* **2012**, *111-112*, 445-455.
(13) Dhillon, P. S.; Harold, M. P.; Wang, D.; Kumar, A.; Joshi, S. Y. Enhanced transport in washcoated monoliths: Application to selective lean $NO_x$ reduction and ammonia oxidation. *Chem. Eng. J.* **2019**, *377*, 119734.
(14) Gonzalez, J. D.; Shojaee, K.; Haynes, B. S.; Montoya, A. The effect of surface coverage on $N_2$, NO and $N_2O$ formation over Pt(111). *Phys. Chem. Chem. Phys.* **2018**, *20* (39), 25314-25323.
(15) Novell-Leruth, G.; Valcárcel, A.; Clotet, A.; Ricart, J. M.; Pérez-Ramírez, J. DFT characterization of adsorbed $NH_x$ species on Pt(100) and Pt(111) surfaces. *J. Phys. Chem. B* **2005**, *109* (38), 18061-18069.
(16) van Santen, R. A. Complementary structure sensitive and insensitive catalytic relationships. *Acc. Chem. Res.* **2009**, *42* (1), 57-66.
(17) Ma, H.; Schneider, W. F. Structure- and temperature-dependence of Pt-catalyzed ammonia oxidation rates and selectivities. *ACS Catal.* **2019**, *9* (3), 2407-2414.
(18) Baerns, M.; Imbihl, R.; Kondratenko, V. A.; Kraehnert, R.; Offermans, W. K.; van Santen, R. A.; Scheibe, A. Bridging the pressure and material gap in the catalytic ammonia oxidation: structural and catalytic properties of different platinum catalysts. *J. Catal.* **2005**, *232* (1), 226-238.
(19) Günther, S.; Scheibe, A.; Bluhm, H.; Haevecker, M.; Kleimenov, E.; Knop-Gericke, A.; Schlogl, R.; Imbihl, R. *In situ* X-ray photoelectron spectroscopy of catalytic ammonia oxidation over a Pt(533) surface. *J. Phys. Chem. C* **2008**, *112* (39), 15382-15393.
(20) Bradley, J. M.; Hopkinson, A.; King, D. A. A molecular beam study of ammonia adsorption on Pt{100}. *Surf. Sci.* **1997**, *371* (2-3), 255-263.
(21) Imbihl, R.; Scheibe, A.; Zeng, Y. F.; Günther, S.; Kraehnert, R.; Kondratenko, V. A.; Baerns, M.; Offermans, W. K.; Jansen, A. P. J.; van Santen, R. A. Catalytic ammonia oxidation on platinum: mechanism and catalyst restructuring at high and low pressure. *Phys. Chem. Chem. Phys.* **2007**, *9* (27), 3522-3540.

(22) Zeng, Y. F.; Imbihl, R. Structure sensitivity of ammonia oxidation over platinum. *J. Catal.* **2009**, *261* (2), 129-136.
(23) Pérez-Ramírez, J.; Kondratenko, E. V.; Kondratenko, V. A.; Baerns, M. Selectivity-directing factors of ammonia oxidation over PGM gauzes in the Temporal Analysis of Products reactor: Secondary interactions of $NH_3$ and NO. *J. Catal.* **2005**, *229* (2), 303-313.
(24) Pérez-Ramírez, J.; Kondratenko, E. V.; Kondratenko, V. A.; Baerns, M. Selectivity-directing factors of ammonia oxidation over PGM gauzes in the Temporal Analysis of Products reactor: Primary interactions of $NH_3$ and $O_2$. *J. Catal.* **2004**, *227* (1), 90-100.
(25) Pérez-Ramírez, J.; Kondratenko, E. V.; Novell-Leruth, G.; Ricart, J. M. Mechanism of ammonia oxidation over PGM (Pt, Pd, Rh) wires by temporal analysis of products and density functional theory. *J. Catal.* **2009**, *261* (2), 217-223.
(26) Kraehnert, R.; Baerns, M. Kinetics of ammonia oxidation over Pt foil studied in a micro-structured quartz-reactor. *Chem. Eng. J.* **2008**, *137* (2), 361-375.
(27) Rebrov, E. V.; de Croon, M.; Schouten, J. C. Development of the kinetic model of platinum catalyzed ammonia oxidation in a microreactor. *Chem. Eng. J.* **2002**, *90* (1-2), 61-76.
(28) Sobczyk, D. P.; van Grondelle, J.; Thune, P. C.; Kieft, I. E.; de Jong, A. M.; van Santen, R. A. Low-temperature ammonia oxidation on platinum sponge studied with positron emission profiling. *J. Catal.* **2004**, *225* (2), 466-478.
(29) Schäffer, J.; Kondratenko, V. A.; Steinfeldt, N.; Sebek, M.; Kondratenko, E. V. Highly selective ammonia oxidation to nitric oxide over supported Pt nanoparticles. *J. Catal.* **2013**, *301*, 210-216.
(30) Sobczyk, D. P.; Hensen, E. J. M.; de Jong, A. M.; van Santen, R. A. Low-temperature ammonia oxidation over Pt/gamma-alumina: the influence of the alumina support. *Top. Catal.* **2003**, *23* (1-4), 109-117.
(31) Slavinskaya, E. M.; Kibis, L. S.; Stonkus, O. A.; Svintsitskiy, D. A.; Stadnichenko, A. I.; Fedorova, E. A.; Romanenko, A. V.; Marchuk, V.; Doronkin, D. E.; Boronin, A. I. The effects of platinum dispersion and Pt state on catalytic properties of $Pt/Al_2O_3$ in $NH_3$ oxidation. *ChemCatChem* **2021**, *13* (1), 313-327.
(32) Svintsitskiy, D. A.; Kibis, L. S.; Stadnichenko, A. I.; Slavinskaya, E. M.; Romanenko, A. V.; Fedorova, E. A.; Stonkus, O. A.; Doronkin, D. E.; Marchuk, V.; Zimina, A.; Casapu, M.; Grunwaldt, J.-D.; Boronin, A. I. Insight into the nature of active species of $Pt/Al_2O_3$ catalysts for low temperature $NH_3$ oxidation. *ChemCatChem* **2020**, *12* (3), 867-880.
(33) Ghosh, R. S.; Dhillon, P. S.; Harold, M. P.; Wang, D. Kinetics of $NH_3$ oxidation on $Pt/Al_2O_3$: Rate enhancement and $NH_3$ inhibition. *Chem. Eng. J.* **2021**, *417*, 128273.
(34) Wang, C.; Ren, D.; Harle, G.; Qin, Q.; Guo, L.; Zheng, T.; Yin, X.; Du, J.; Zhao, Y. Ammonia removal in selective catalytic oxidation: Influence of catalyst structure on the nitrogen selectivity. *J. Hazard. Mater.* **2021**, *416*, 125782.
(35) Sun, M.; Liu, J.; Song, C.; Ogata, Y.; Rao, H.; Zhao, X.; Xu, H.; Chen, Y. Different reaction mechanisms of ammonia oxidation reaction on $Pt/Al_2O_3$ and $Pt/CeZrO_2$ with various Pt states. *ACS Appl. Mater. Interfaces* **2019**, *11* (26), 23102-23111.
(36) Kibis, L. S.; Svintsitskiy, D. A.; Stadnichenko, A. I.; Slavinskaya, E. M.; Romanenko, A. V.; Fedorova, E. A.; Stonkus, O. A.; Svetlichnyi, V. A.; Fakhrutdinova, E. D.; Vorokhta, M.; Smid, B.; Doronkin, D. E.; Marchuk, V.; Grunwaldt, J.-D.; Boronin, A. I. *In situ* probing of $Pt/TiO_2$ activity in low-temperature ammonia oxidation. *Catal. Sci. Technol.* **2021**, *11* (1), 250-263.
(37) Lin, M. Y.; An, B. X.; Takei, T.; Shishido, T.; Ishida, T.; Haruta, M.; Murayama, T. Features of Nb2O5 as a metal oxide support of Pt and Pd catalysts for selective catalytic oxidation of NH3 with high N-2 selectivity. *J. Catal.* **2020**, *389*, 366-374.
(38) Ivashenko, O.; Johansson, N.; Pettersen, C.; Jensen, M.; Zheng, J.; Schnadt, J.; Sjastad, A. O. How surface species drive product distribution during ammonia oxidation: An STM and *operando* APXPS Study. *ACS Catal.* **2021**, *11* (13), 8261-8273.
(39) Kraehnert, R.; Baerns, M. Morphology changes of Pt-foil catalyst induced by temperature-controlled ammonia oxidation near atmospheric pressure. *Appl. Catal. A Gen.* **2007**, *327* (1), 73-81.
(40) Ostermaier, J. J.; Katzer, J. R.; Manogue, W. H. Crystallite size effects in low-temperature oxidation of ammonia over supported platinum. *J. Catal.* **1974**, *33* (3), 457-473.

(41) Ostermaier, J. J.; Katzer, J. R.; Manogue, W. H. Platinum catalyst deactivation in low-temperature ammonia oxidation reactions. 1. Oxidation of ammonia by molecular oxygen. *J. Catal.* **1976**, *41* (2), 277-292.
(42) Hansen, T. K. Development of new diesel oxidation and $NH_3$ slip catalysts. PhD thesis, Technical University of Denmark, 2017. https://orbit.dtu.dk/en/publications/development-of-new-diesel-oxidation-and-nhsub3sub-slip-catalysts (accessed on Dec 11, 2023).
(43) Machida, M.; Tokudome, Y.; Maeda, A.; Kuzuhara, Y.; Hirakawa, T.; Sato, T.; Yoshida, H.; Ohyama, J.; Fujii, K.; Ishikawa, N. Nanometric platinum overlayer to catalyze $NH_3$ oxidation with high turnover frequency. *ACS Catal.* **2020**, *10* (8), 4677-4685.
(44) Rebrov, E. V.; de Croon, M.; Schouten, J. C. A kinetic study of ammonia oxidation on a Pt catalyst in the explosive region in a microstructured reactor/heat-exchanger. *Chem. Eng. Res. Des.* **2003**, *81* (A7), 744-752.
(45) Colombo, M.; Nova, I.; Tronconi, E.; Schmeißer, V.; Bandl-Konrad, B.; Zimmermann, L. Experimental and modeling study of a dual-layer (SCR+PGM) $NH_3$ slip monolith catalyst (ASC) for automotive SCR aftertreatment systems. Part 1. Kinetics for the PGM component and analysis of SCR/PGM interactions. *Appl. Catal. B* **2013**, *142-143*, 861-876.
(46) Whiting, G. T.; Meirer, F.; Weckhuysen, B. M. *Operando* EXAFS and XANES of Catalytic Solids and Related Materials. In *XAFS Techniques for Catalysts, Nanomaterials, and Surfaces*, Iwasawa, Y., Asakura, K., Tada, M. Eds.; Springer International Publishing, 2017; pp 167-191.
(47) Boubnov, A.; Dahl, S.; Johnson, E.; Molina, A. P.; Simonsen, S. B.; Cano, F. M.; Helveg, S.; Lemus-Yegres, L. J.; Grunwaldt, J.-D. Structure–activity relationships of $Pt/Al_2O_3$ catalysts for CO and NO oxidation at diesel exhaust conditions. *Appl. Catal. B* **2012**, *126*, 315-325.
(48) Decarolis, D.; Clark, A. H.; Pellegrinelli, T.; Nachtegaal, M.; Lynch, E. W.; Catlow, C. R. A.; Gibson, E. K.; Goguet, A.; Wells, P. P. Spatial profiling of a $Pd/Al_2O_3$ catalyst during selective ammonia oxidation. *ACS Catal.* **2021**, *11* (4), 2141-2149.
(49) Maurer, F.; Jelic, J.; Wang, J.; Gänzler, A.; Dolcet, P.; Wöll, C.; Wang, Y.; Studt, F.; Casapu, M.; Grunwaldt, J.-D. Tracking the formation, fate and consequence for catalytic activity of Pt single sites on $CeO_2$. *Nat. Catal.* **2020**, *3* (10), 824-833.
(50) Marchuk, V.; Huang, X.; Grunwaldt, J.-D.; Doronkin, D. E. Structure sensitivity of alumina- and zeolite-supported platinum ammonia slip catalysts. *Catal. Sci. Technol.* **2023**, *13*, 2946-2965.
(51) Jentys, A. Estimation of mean size and shape of small metal particles by EXAFS. *Phys. Chem. Chem. Phys.* **1999**, *1* (17), 4059-4063.
(52) Weisz, P. B.; Prater, C. D. *Advances in Catalysis*; Academic, 1954.
(53) Bornmann, B.; Kläs, J.; Müller, O.; Luetzenkirchen-Hecht, D.; Frahm, R. The quick EXAFS setup at beamline P64 at PETRA III for up to 200 spectra per second. *AIP Conf. Proc.* **2019**, *2054* (1), 040008.
(54) Clark, A. H.; Imbao, J.; Frahm, R.; Nachtegaal, M. ProQEXAFS: a highly optimized parallelized rapid processing software for QEXAFS data. *J. Synchrotron Radiat.* **2020**, *27*, 551-557.
(55) Windig, W.; Markel, S. Simple-to-use interactive self-modeling mixture analysis of FTIR microscopy data. *J. Mol. Struct.* **1993**, *292*, 161-170.
(56) Jaumot, J.; de Juan, A.; Tauler, R. MCR-ALS GUI 2.0: New features and applications. *Chemom. Intell. Lab. Syst.* **2015**, *140*, 1-12.
(57) Grunwaldt, J.-D.; Caravati, M.; Hannemann, S.; Baiker, A. X-ray absorption spectroscopy under reaction conditions: suitability of different reaction cells for combined catalyst characterization and time-resolved studies. *Phys. Chem. Chem. Phys.* **2004**, *6* (11), 3037-3047.
(58) Kresse, G.; Furthmüller, J. Efficient iterative schemes for ab initio total-energy calculations using a plane-wave basis set. *Phys. Rev. B* **1996**, *54* (16), 11169-11186.
(59) Kresse, G.; Furthmüller, J. Efficiency of ab-initio total energy calculations for metals and semiconductors using a plane-wave basis set. *Comput. Mater. Sci.* **1996**, *6* (1), 15-50.
(60) Mortensen, J. J.; Kaasbjerg, K.; Frederiksen, S. L.; Nørskov, J. K.; Sethna, J. P.; Jacobsen, K. W. Bayesian Error Estimation in Density-Functional Theory. *Phys. Rev. Lett.* **2005**, *95* (21), 216401.

(61) Wellendorff, J.; Lundgaard, K. T.; Møgelhøj, A.; Petzold, V.; Landis, D. D.; Nørskov, J. K.; Bligaard, T.; Jacobsen, K. W. Density functionals for surface science: Exchange-correlation model development with Bayesian error estimation. *Phys. Rev. B* **2012**, *85* (23), 235149.
(62) Blöchl, P. E. Projector augmented-wave method. *Phys. Rev. B* **1994**, *50* (24), 17953-17979.
(63) Kresse, G.; Joubert, D. From ultrasoft pseudopotentials to the projector augmented-wave method. *Phys. Rev. B* **1999**, *59* (3), 1758-1775.
(64) Marchuk, V.; Sharapa, D. I.; Grunwaldt, J.-D.; Doronkin, D. E. Atomic coordinates of DFT-optimized Pt structures with O, N, and $NH_x$ species in surface or interstitial locations. *KITopen.* Karlsruhe Institute of Technology, 2023. doi: 10.35097/1764.
(65) Rehr, J. J.; Kas, J. J.; Vila, F. D.; Prange, M. P.; Jorissen, K. Parameter-free calculations of X-ray spectra with FEFF9. *Phys. Chem. Chem. Phys.* **2010**, *12* (21), 5503-5513.
(66) Safonova, O. V.; Tromp, M.; van Bokhoven, J. A.; de Groot, F. M. F.; Evans, J.; Glatzel, P. Identification of CO adsorption sites in supported Pt catalysts using high-energy-resolution fluorescence detection X-ray spectroscopy. *J. Phys. Chem. B* **2006**, *110* (33), 16162-16164.
(67) Casapu, M.; Fischer, A.; Gänzler, A. M.; Popescu, R.; Crone, M.; Gerthsen, D.; Turk, M.; Grunwaldt, J.-D. Origin of the normal and inverse hysteresis behavior during CO oxidation over $Pt/Al_2O_3$. *ACS Catal.* **2017**, *7* (1), 343-355.
(68) Gänzler, A. M.; Casapu, M.; Doronkin, D. E.; Maurer, F.; Lott, P.; Glatzel, P.; Votsmeier, M.; Deutschmann, O.; Grunwaldt, J.-D. Unravelling the different reaction pathways for low temperature CO oxidation on $Pt/CeO_2$ and $Pt/Al_2O_3$ by spatially resolved structure–activity correlations. *J. Phys. Chem. Lett.* **2019**, *10* (24), 7698-7705.
(69) Johánek, V.; Václavu, M.; Matolínová, I.; Khalakhan, I.; Haviar, S.; Matolín, V. High low-temperature CO oxidation activity of platinum oxide prepared by magnetron sputtering. *Appl. Surf. Sci.* **2015**, *345*, 319-328.
(70) Doronkin, D. E.; Kuriganova, A. B.; Leontyev, I. N.; Baier, S.; Lichtenberg, H.; Smirnova, N. V.; Grunwaldt, J. D. Electrochemically synthesized $Pt/Al_2O_3$ oxidation catalysts. *Catal. Lett.* **2016**, *146* (2), 452-463.
(71) Chen, L. X.; McCann, J. P.; Tait, S. L. A re-examination of the catalyst activation and temperature hysteresis in methane combustion on $Pt/Al_2O_3$. *Appl. Catal. A Gen.* **2018**, *549*, 19-30.
(72) Chou, C. P.; Chen, J. Y.; Evans, G. H.; Winters, W. S. Numerical studies of methane catalytic combustion inside a monolith honeycomb reactor using multi-step surface reactions. *Combust. Sci. Technol.* **2000**, *150* (1-6), 27-57.
(73) Griffin, T. A.; Pfefferle, L. D. Gas-phase and catalytic ignition of methane and ethane in air over platinum. *AlChE J.* **1990**, *36* (6), 861-870.
(74) Zhang, L.; He, H. Mechanism of selective catalytic oxidation of ammonia to nitrogen over $Ag/Al_2O_3$. *J. Catal.* **2009**, *268* (1), 18-25.
(75) Toops, T. J.; Smith, D. B.; Epling, W. S.; Parks, J. E.; Partridge, W. P. Quantified $NO_x$ adsorption on Pt/K/gamma-$Al_2O_3$ and the effects of $CO_2$ and $H_2O$. *Appl. Catal. B* **2005**, *58* (3), 255-264.
(76) Bradley, J. M.; Hopkinson, A.; King, D. A. Control of a biphasic surface reaction by oxygen coverage: The catalytic oxidation of ammonia over Pt{100}. *J. Phys. Chem.* **1995**, *99* (46), 17032-17042.
(77) Mieher, W. D.; Ho, W. Thermally activated oxidation of $NH_3$ on Pt(111): intermediate species and reaction mechanisms. *Surf. Sci.* **1995**, *322* (1), 151-167.
(78) Weststrate, C. J.; Bakker, J. W.; Rienks, E. D. L.; Vinod, C. P.; Matveev, A. V.; Gorodetskii, V. V.; Nieuwenhuys, B. E. Ammonia oxidation on Pt(410). *J. Catal.* **2006**, *242* (1), 184-194.
(79) Singh, J.; Alayon, E. M. C.; Tromp, M.; Safonova, O. V.; Glatzel, P.; Nachtegaal, M.; Frahm, R.; van Bokhoven, J. A. Generating highly active partially oxidized platinum during oxidation of carbon monoxide over $Pt/Al_2O_3$: *In situ*, time-resolved, and high-energy-tesolution X-ray absorption spectroscopy. *Angew. Chem. Int. Ed.* **2008**, *47* (48), 9260-9264.
(80) Novell-Leruth, G.; Valcárcel, A.; Pérez-Ramírez, J.; Ricart, J. M. Ammonia dehydrogenation over platinum-group metal surfaces. Structure, stability, and reactivity of adsorbed $NH_x$ species. *J. Phys. Chem. C* **2007**, *111* (2), 860-868.

(81) Parker, D. H.; Bartram, M. E.; Koel, B. E. Study of high coverages of atomic oxygen on the Pt(111) surface. *Surf. Sci.* **1989**, *217* (3), 489-510.
(82) Miller, D. J.; Öberg, H.; Kaya, S.; Sanchez Casalongue, H.; Friebel, D.; Anniyev, T.; Ogasawara, H.; Bluhm, H.; Pettersson, L. G. M.; Nilsson, A. Oxidation of Pt(111) under near-ambient conditions. *Phys. Rev. Lett.* **2011**, *107* (19), 195502.
(83) Parkinson, C. R.; Walker, M.; McConville, C. F. Reaction of atomic oxygen with a Pt(111) surface: chemical and structural determination using XPS, CAICISS and LEED. *Surf. Sci.* **2003**, *545* (1), 19-33.
(84) Devarajan, S. P.; Hinojosa, J. A.; Weaver, J. F. STM study of high-coverage structures of atomic oxygen on Pt(111): p(2×1) and Pt oxide chain structures. *Surf. Sci.* **2008**, *602* (19), 3116-3124.
(85) Butcher, D. R.; Grass, M. E.; Zeng, Z.; Aksoy, F.; Bluhm, H.; Li, W.-X.; Mun, B. S.; Somorjai, G. A.; Liu, Z. *In situ* oxidation study of Pt(110) and its interaction with CO. *J. Am. Chem. Soc.* **2011**, *133* (50), 20319-20325.
(86) Wang, J. G.; Li, W. X.; Borg, M.; Gustafson, J.; Mikkelsen, A.; Pedersen, T. M.; Lundgren, E.; Weissenrieder, J.; Klikovits, J.; Schmid, M.; Hammer, B.; Andersen, J. N. One-dimensional $PtO_2$ at Pt steps: formation and reaction with CO. *Phys. Rev. Lett.* **2005**, *95* (25), 256102.
(87) van Spronsen, M. A.; Frenken, J. W. M.; Groot, I. M. N. Observing the oxidation of platinum. *Nat. Commun.* **2017**, *8* (1), 429.
(88) Vovk, E. I.; Kalinkin, A. V.; Smirnov, M. Y.; Klembovskii, I. O.; Bukhtiyarov, V. I. XPS study of stability and reactivity of oxidized Pt nanoparticles supported on $TiO_2$. *J. Phys. Chem. C* **2017**, *121* (32), 17297-17304.
(89) Smirnov, M. Y.; Kalinkin, A. V.; Bukhtiyarov, V. I. X-ray photoelectron spectroscopic study of the interaction of supported metal catalysts with $NO_x$. *J. Struct. Chem.* **2007**, *48* (6), 1053-1060.
(90) Gland, J. L.; Sexton, B. A.; Fisher, G. B. Oxygen interactions with the Pt(111) surface. *Surf. Sci.* **1980**, *95* (2), 587-602.
(91) Bashlakov, D. L.; Juurlink, L. B. F.; Koper, M. T. M.; Yanson, A. I. Subsurface oxygen on Pt(111) and its reactivity for CO oxidation. *Catal. Lett.* **2012**, *142* (1), 1-6.
(92) Gu, Z.; Balbuena, P. B. Absorption of atomic oxygen into subsurfaces of Pt(100) and Pt(111): Density functional theory study. *J. Phys. Chem. C* **2007**, *111* (27), 9877-9883.
(93) Gu, Z.; Balbuena, P. B. Chemical environment effects on the atomic oxygen absorption into Pt(111) subsurfaces. *J. Phys. Chem. C* **2007**, *111* (46), 17388-17396.